Electrochimica Acta 315 (2019) 84–93

Contents lists available at ScienceDirect

Electrochimica Acta

journal homepage: www.elsevier.com/locate/electacta

Ferrocene self assembled monolayer as a redox mediator for triggering ion transfer across nanometer-sized membranes

Maria Cuartero [a], Lijun Chai [a], Biaobiao Zhang [a], Roland De Marco [b, c, d], Gastón A. Crespo [a, *]

[a] Department of Chemistry, KTH Royal Institute of Technology, 10044, Stockholm, Sweden
[b] Faculty of Science, Health, Education and Engineering, University of the Sunshine Coast, 90s Sippy Downs Drive, Sippy Downs, Queensland, 4556, Australia
[c] School of Chemistry and Molecular Biosciences, The University of Queensland, Brisbane, Queensland, 4072, Australia
[d] Fuels and Energy Technology Institute, Curtin University, Perth, WA, 6102, Australia

ARTICLE INFO

Article history:
Received 10 April 2019
Received in revised form
17 May 2019
Accepted 17 May 2019
Available online 20 May 2019

Keywords:
Voltammetry membranes
Self-assembled monolayer
Ion transfer
Ionophores

ABSTRACT

Modulation of ion-transfer processes across nanometer-sized voltammetry membranes by ferrocene-based self-assembled monolayer on regular glassy carbon electrode is herein demonstrated. The composition of the membrane is advantageously tuned to promote either cation or anion transfer: the presence of an exchangeable cation results in cation transfer, whereas a lipophilic salt induces anion transfer through the fulfilment of the electroneutrality of the system. When an anodic scan oxidizes ferrocene moieties in the monolayer, these are stabilized by the pairing of lipophilic anions present in the membrane. As a result, either, hydrophilic cations present in the membrane are expelled into the solution or anions enter from the solution generating hence reversible and voltammetric waves for these transfers. The use of a redox active monolayer rather than a conducting polymer film or a redox active compound into the membrane overcomes a number of drawbacks previously manifested by these systems. The confinement of the redox process in a thin film at the immediate vicinity of the membrane allows to avoid the need of elevated number of redox moieties to be sued in the membrane, therefore suppressing its acute leaching and being compatible with the incorporation of both cation and anion ionophores for the first time. In this sense, assisted transfer of lithium and chloride are shown as proof-of-concept. Here, the peak potential of the associated voltammetric waves shifts according to the Nernst equation, in analogy to potentiometric sensors. Analytical detection of lithium and chloride ions in real samples is additionally presented.

1. Introduction

Over the past decade, the conceiving of ion-transfer processes across ion-selective membranes has significantly evolved. Accordingly, traditional measurements at zero current (i.e., potentiometry) have been superseded by dynamic electrochemistry, in cases where the limit of detection, selectivity and/or re-calibration frequency limit the final analytical application of conventional potentiometric sensors [1–3]. In this context, Bond pioneered the modulation of ion transfer by controlling the oxidation state of a redox film (made of 7,7,8,8-tetracyanoquinodimethane, $TCNQ^{0/-}$) beneath a permselective membrane (Nafion) [4,5]. In the observed voltammograms, it was shown that the peak potential displayed a Nernstian dependency at increasing ion concentration.

This concept was taken one step further with the use of ion-selective membranes backside contacted with the conducting polymers poly(3,4-ethylenedioxythiophene) (PEDOT) and poly(3-octylthiophene) (POT) [6–10]. Here, the driving force for ion transfer had its root in the maintenance of electroneutrality of the system while the redox mediator introduced charge through electrochemical oxidation. For instance, in the case of a membrane based on a cation exchanger (Na^+R^-) with a POT underlayer, POT is gradually oxidized to POT^+ using cyclic voltammetry, with POT^+ stabilized by R^- in the membrane with the concomitant release of Na^+ to the solution [11]. The peak potential of the wave associated with this cation transfer shifts to more positive values at increasing cation concentrations in accordance with the Nernst equation, as introduced by Bond [4,11].

* Corresponding author.
E-mail address: gacp@kth.se (G.A. Crespo).

https://doi.org/10.1016/j.electacta.2019.05.091

Later, the use of a single nanometer-thick membrane (ca. 250 nm of thickness measured by ellipsometry) doped with up to three ionophores allowed for an unprecedented detection of multiple cations (i.e., lithium, sodium and potassium) in a complex matrix such as undiluted blood [12,13]. Besides the selectivity pattern inherent to each ionophore, the width of the voltammetry peaks marks the limit of detection of the sensor for ion analyses. Notably, it was already demonstrated that peaks as wider as 210 mV are observed with POT-based electrodes because of the film oxidation/reduction does not occur through an ideal one-electron-transfer process [11].

The incorporation of a redox active molecule (based on a metallic center) directly in the membrane emerged aiming at a substitution of the POT underlayer, thus providing mediators with well-defined redox behavior [14–18]. The first trials were based on ferrocene (Fc) derivatives [19]. Nevertheless, these membranes presented a strong chloride interference. More recently, membranes comprising Os-based compounds [16] and helicenes [17,18] have shown promising voltammetric properties, but require the addition of a large amount of redox compound in the membrane. This is incompatible with the incorporation of any ionophore, and often leads to a marked leaching of the compound from the thin membrane [17].

Up to now, the aforesaid strategies for the mediation of ion-transfer processes across thin membranes possess distinct advantages and drawbacks (i.e. the redox behavior of the mediator is not well-defined, compounds' leaching from the membrane, chloride interference and level of affordability of the ionophore incorporation). So that, there is an urgent need to provide a new strategy that is capable of overcoming these issues. Some clues may arise after inspecting the history of the development of the all-solid-state concept for electrodes based on ion-selective membranes.

Despite the widespread use of conducting polymers as a preferred option in this kind of sensors, other materials have demonstrated effective ion-to-electron transduction during the last decade (e.g. carbon-based structures [20–23], nanomaterials [24,25], redox active monolayers [26,27], Prussian blue films [28], silver complexes [29] and redox pairs [30,31], among others). While their success has been realised in potentiometric detection [32], these materials have not been exploited rigorously when the membrane is interrogated using a dynamic electrochemical technique. Specifically, redox active monolayers are attractive as ion transfer mediators with voltammetrically controlled membranes.

Pretsch and co-workers were the very first to explore redox-active self-assembled monolayers (SAMs) [based on fullerene or tetrathiafulvalene] as solid contacts on gold electrodes [26]. The authors found that the lipophilicity of the monolayer hindered the formation of an aqueous layer at the membrane|electrode surface, resulting also in a stronger adhesion of membranes based on different polymers, such as polyvinylchloride (PVC) or polyurethane (PU). The use of mixed monolayers also incorporating an n-octanethiol film allowed for an improvement in the stability of these devices, with low long-term potential drift (85 $\mu V\,h^{-1}$), as well as a compatibility with thinner selective membranes than those used traditionally in potentiometry (10 μm *versus* 200–500 μm) [27]. More recently, the use of other kinds of SAMs with underpinned polymeric ion-selective membranes in potentiometric (Fc on gold [33] and on silicon-based chips [34]) as well as voltammetric modes (Fc on silicon [35]) have been presented. This latter electrode was exclusively used in the light-addressable sensing of extracellular potassium.

In this paper, we propose the use of a Fc monolayer on glassy carbon (GC) electrode as redox mediator of ion-transfer processes across nanometer-sized membranes as an alternative to the use of POT [13] or redox compounds added to the membrane [14,16–18]. In principle, the immobilization of the redox molecule (i.e. Fc) as a monolayer at the buried interface of the membrane|electrode, is expected to solve the aforementioned leaching issue. In addition, the confinement of the oxidation of the monolayer (from Fc^0 to Fc^+) in the close vicinity of the electrode surface will reduce the demand for a large amount of reactive metallic center for effective ion transfer, so this approach is more compatible with and better suited to the incorporation of ionophores into membranes. Finally, chloride interference on the Fc electrochemistry is ameliorated since the electrode does not involve a direct stabilization of the oxidized monolayer (Fc^+) by chloride ions entering from the solution. As a result, it is expected that the proposed system would be compatible with both cation and anion detection.

2. Experimental

2.1. Preparation of glassy carbon electrode modified with ferrocene monolayer

Fig. S1 presents the approach used for the modification of commercial glassy carbon (GC) electrodes with ferrocene (Fc) monolayer [36]. First, The reductive electrodeposition of diazonium salts on GC electrode was performed in a deaerated solution (with argon) of 0.1 M HCl solution containing 1.5 mM of 4-azidobenzene diazonium tetrafluoroborate ($[N_3{-}C_6H_4{-}N_2]^+BF_4^-$), which was synthetized as reported elsewhere [37], at ice-water bath. The working electrode (GC) was polarized at −0.6 V for 1 min with standard hydrogen electrode and platinum wire used as reference and counter electrodes, respectively. Subsequently, the azide|GC electrodes were thoroughly washed with Milli-Q water and ethanol to remove any physically adsorbed species. Thereafter, they were immersed in a Milli-Q water solution containing $CuSO_4$ (10 mM), L-ascorbic acid (10 mM) and ethynilferrocene (10 μM) at room temperature for overnight. The Fc|azide|GC electrode were thoroughly rinsed with Milli-Q water and ethanol to remove any physisorbed species.

2.2. Modification of Fc monolayers with nanometer-sized membranes

A volume of 25 μL of the corresponding membrane cocktail was spin coated onto the Fc-modified electrode (1500 rpm). Table S1 shows the composition of the membrane cocktails used throughout the paper. In the case of membranes containing PVC, a dilution of the cocktail was first accomplished by mixing 50 μL of the original cocktail with 150 μL of THF. Regarding PU membranes, no dilution was used. With the described procedure, membranes of ca.250 nm of thickness are provided, as already demonstrated in our previous works [12]. The prepared electrodes were electrochemically interrogated always against a double-junction Ag/AgCl/3 M KCl/1 M LiOAc reference electrode (6.0726.100 model, Metrohm Nordic) and a platinum electrode (6.0331.010 model, Metrohm Nordic) in a three-electrode cell. The reader is referred to the Supporting Information for more details.

3. Results and discussion

3.1. Characterization of the Fc monolayer

Firstly, the electrochemical behavior of the Fc monolayer was investigated using cyclic voltammetry. Fig. 1a presents voltammograms in ferrocyanide/ferricyanide ($K_3Fe(CN)_6/K_4Fe(CN)_6$) solution before and after the modification of the GC electrode with the azide-intermediate (i.e., bare GC electrode *versus* azide|GC electrode). As expected, the bare GC electrode showed well-defined

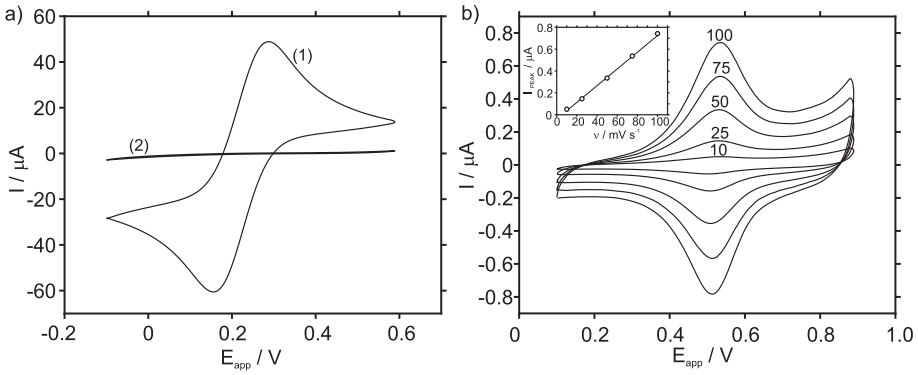

Fig. 1. (a) Voltammograms for (1) bare GC electrode and (2) azide|GC electrode in 0.1 M $K_3Fe(CN)_6$/0.1 M $K_4Fe(CN)_6$ solution. Scan rate = 100 mV s^{-1}. (b) Voltammograms using Fc|azide|GC electrode in 0.1 M $TBAPF_6$/ACN solution at increasing scan rates. Inset: peak current *versus* scan rate.

and reversible peaks for the Fe^{2+}/Fe^{3+} redox couple (Fig. 1a, curve 1), whereas no response is displayed after the introduction of the azide compound (curve 2). Thus, the GC surface is, in principle, totally blocked by the azide layer, with electron transfer for the oxidation/reduction of Fe^{2+}/Fe^{3+} molecules supressed as a result of azide functionalization of the surface.

When the Fc moieties are incorporated to the azide layer (Fc|azide|GC electrode), these can be oxidized/reduced in presence of certain anions able to reversibly dope the oxidized Fc^+. In this sense, Fig. 1b shows the redox behavior of the Fc monolayer in organic solution containing PF_6^- anion. It is evident that anodic scanning oxidizes Fc to Fc^+ that is stabilized by PF_6^-. This is manifested by a Gaussian peak that is totally reversible and reproducible on continuous scanning (Fig. S2a). Thus, the integrated charge for anodic and cathodic peaks (0.9003 and 0.9184 μC respectively) only differs by 2%. The width at half peak ($W_{1/2}$) is around 160 mV at 100 mV s^{-1}, noting that for a one electron transfer process a $W_{1/2}$ of 90 mV is expected with a bulk material rather than a SAM. This is in agreement with the general behavior of a redox active monolayer that presents a certain charge distribution over its entire surface [38,39]. As a result, the monolayer does not act following a purely one electron transfer process. In addition, the $W_{1/2}$ values that are either larger or smaller than the theoretical value have been attributed to electrostatic effects incurred by neighboring charged species [40].

The peak current increases linearly with scan rate (Fig. 1b) since the electrochemical oxidation/reduction of the monolayer is a surface confined process [41,42]. On the other hand, the peak separation ($|E_{p,c} - E_{p,a}|$) is reduced from 25 mV at 100 mV s^{-1} down to zero while decreasing the scan rate, which was already observed with other Fc monolayers [40]. The redox potential (E^0) associated with the SAM film, which is calculated from the average of the anodic and cathodic peak potentials, was determined to be 525 mV (versus the Ag/AgCl reference electrode) and, as expected for a SAM, it changes very little at different scan rates.

GC electrodes modified with Fc monolayer can be used for several days after preparation, if they are stored in the same solution as the one used in the last step of the SAM synthesis (i.e., $CuSO_4$, L-ascorbic acid and EtFc). Accordingly, after two weeks of electrode preparation, the behavior of the Fc monolayer in $TBAPF_6$ solution remained rather constant (Fig. S2b). Other suitable options involve a preparation of the azide layer and storage of the azide modified electrode in the absence of dust and light followed by clicking of the Fc molecules (overnight conditioning in EtFc) prior to utilization. After two weeks of the preparation of the azide layer, the behavior of the Fc monolayer in $TBAPF_6$ solution does not change. Otherwise, Fc|azide|GC electrodes function reproducibly after a couple of days if they are stored in the absence of light once they have been rinsed/cleaned.

It is worth mentioning that the recorded current during the oxidation of the Fc monolayer begins to grow with the applied potential when this is higher than 0.75 V (*versus* the Ag/AgCl electrode, see Figs. S2a and S2c), which has been attributed to the capacitance of the SAM film in the "double-layer region" of the associated voltammogram [38]. This behavior of the current manifested in the voltammograms accords with the investigations of Evrard et al. [36], who reported for the first time the synthesis approach of Fc monolayer analogous to the one used in this paper, but also with other types of Fc monolayers [40].

The capacitance of the monolayer film was calculated to be 1.2 μF before the redox peak and 2.3 μF after it (at 220 and 805 mV respectively), according to the following equation:

$$C_{film} = \frac{1}{2}\left|\frac{i_{E,a} - i_{E,c}}{scan\ rate}\right| \quad (1)$$

where $i_{E,a}$ and $i_{E,c}$ are anodic and cathodic charging currents measured at a potential E in the double-layer region, respectively. This marked increase in the double-layer capacitance when the Fc is fully oxidized is in agreement with previous reports (for $E_{app} > 0.65$ V *versus* the saturated calomel reference electrode) [38]. Hence, the oxidized film is more permeable to ions and, the resultant increase in ion partition coefficient leads to the development of an ionic space charge within the Fc film.

In order to study this phenomenon in more detail, the redox behavior of the Fc monolayer was evaluated within an expanded potential window. The observed peak current decreases and shifts to more positive potentials upon continuous scanning (i.e. the peak potential changed from 530 to 645 mV comparing the first and the 50th scan in Fig. S2c). Indeed, after the 50th scan, the anodic peak becomes a small shoulder on the capacitance signal of the monolayer, while the cathodic peak has disappeared. This behavior points to the alteration of the double-layer capacitance in the Fc SAM in scanning, becoming this more stable and even irreversible, when the SAM film is interrogated at extreme potentials. Moreover, the peak shift to positive potentials may indicate that oxidation of the Fc moieties has become kinetically more unfavorable. In view of these experiments, it is not convenient to scan the Fc|azide|GC electrode at high positive potentials (higher than 0.8 V *versus* the Ag/AgCl reference electrode), so as to eliminate a gradual deterioration of the SAM electrochemistry. As far as the potential window does not exceed a value of 0.8 V, the observed voltammetric peak is totally reproducible, not only between scans (Fig. S2a), but also between electrodes. For example, analyzing a set of ten freshly

prepared Fc|azide|GC electrodes yielded mean absolute deviations of 0.011 μA and 6.72 mV in the peak current and the peak potential of the multiple electrodes, respectively.

The characterization of the Fc monolayer was additionally accomplished by synchrotron radiation-X-ray photoelectron spectroscopy (SR-XPS) and near edge X-ray absorption fine structure (NEXAFS) measurements. The SR-XPS N 1s spectra for azide|GC, Fc|azide|GC electrode and Fc|azide|GC electrode subjected to 100 CVs at an expanded potential window (Fig. 2a, Table S1 and Table S2) reveal −N═N− at about 399.5 eV, $-N^{-}=N^{+}=N$ and $-N=N^{+}=N^{-}$ at about 401 eV and $-N^{-}=N^{+}=N$ and $-N=N^{+}=N^{-}$ at about 404 eV, noting that the coloring of N is indicative of the N atom that had been detected by SR-XPS [43].

In accordance with Coates et al. [44], only a decrease in the 404 eV component (azide|GC) after clicking of the Fc group (Fc|azide|GC) is caused by partial reaction of the azide as a result of steric hindrance at the surface, which impedes the click reaction over the entire surface. On the other hand, the significant decrease in the intensity of the 401 eV and minimal change to the 399.5 eV components are symbolic of the successful clicking of Fc, although not over the entire azide surface.

After 100 CVs at an expanded potential window (from −0.5–1.2 V), Fe in the Fc functionality is totally removed (see the Fe/N atomic ratio in Table S2), which accounts for the complete loss of the reversible Fc/Fc^{+} electrochemistry in this condition (see Fig. S2c). Indeed, the N 1s spectra revert to a similar pattern with the clicked Fc Azide surface whereas the rest of the aliphatic and aromatic N moieties remain intact.

The Fe/N and N/C–N ratios as well as %N1 (i.e., −N═N−), %N2 (i.e., $-N^{-}=N^{+}=N$ and $-N=N^{+}=N^{-}$) and %N3 (i.e., $-N^{-}=N^{+}=N$ and $-N=N^{+}=N^{-}$), as determined using SR-XPS, also provided valuable information (Table S2). Theoretically, the N/C–N ratio for the native azide surface should be 3:1, with the experimental result falling within the bounds of experimental uncertainty (i.e., 2.6 ± 0.7). The clicked Fc azide surface (i.e., 100% of 1,2,3-triazole moiety) will give a theoretical value for N/C–N ratio of 1 (experimental value of 1.7 ± 0.4), with all other clicked Fc azide surfaces yielding similar N/C–N ratios, which is consistent with the previous observation of a surface comprising a mixture of unclicked azide (N/C–N of 3) and 1,2,3-triazole moiety (N/C–N of 1) [viz., about 75% of the 1,2,3-triazole moiety and 25% of azide for a total N/C–N ratio of about 1.5, which is the average of all clicked surfaces. As an example, C 1s and Fe 2p core levels are shown in Fig. S3 for the regular Fc|azide|GC electrode.

The C 1s spectra shows graphitic C at 284.5 eV from GC and adventitious hydrocarbons, C–N at about 285.0 eV from Fc azide and C–OH at approximately 286.5 eV from oxidized GC. The Fe/N ratio in the Fc|azide|GC electrode should be 0.33, but we found a value of 0.41–0.8 for all of the clicked and polarized surfaces (about 150–250% of the expected value). It is worth noting that SR-XPS of the Fe 2p core level at a photon energy giving an electron kinetic energy of 50 eV could not detect any Fe, with the Fe 2p SR-XPS spectrum only observable at an electron kinetic energy of 290 eV (Fig. S3b). The sole detection of Fe with deeper originating photoelectrons at higher kinetic energies suggests an unusual orientation of the monolayer in which the Fc moieties are somehow buried beneath the SAM surface.

Valence band spectroscopy (VBS) of the same samples are presented in Fig. 2b together with a magnification of the density of states (DOS) near to Fermi edge. There are peaks at 6–7 eV, about 9 eV and 13–14 eV that are symbolic of the C 2p states in Fc moieties, C 2p states in C–N and s and p character of the C–N bonds in nitrogenated films [45,46]. In addition, the valence band maximum (VBM) in the DOS near to the Fermi level shifts positively by a few tenths of an eV between the different samples, which is symbolic of upward surface band bending as a consequence of SAM film formation [47].

Fig. 2c and d presents the NEXAFS N 1s and Fe $2p_{3/2}$ for the same

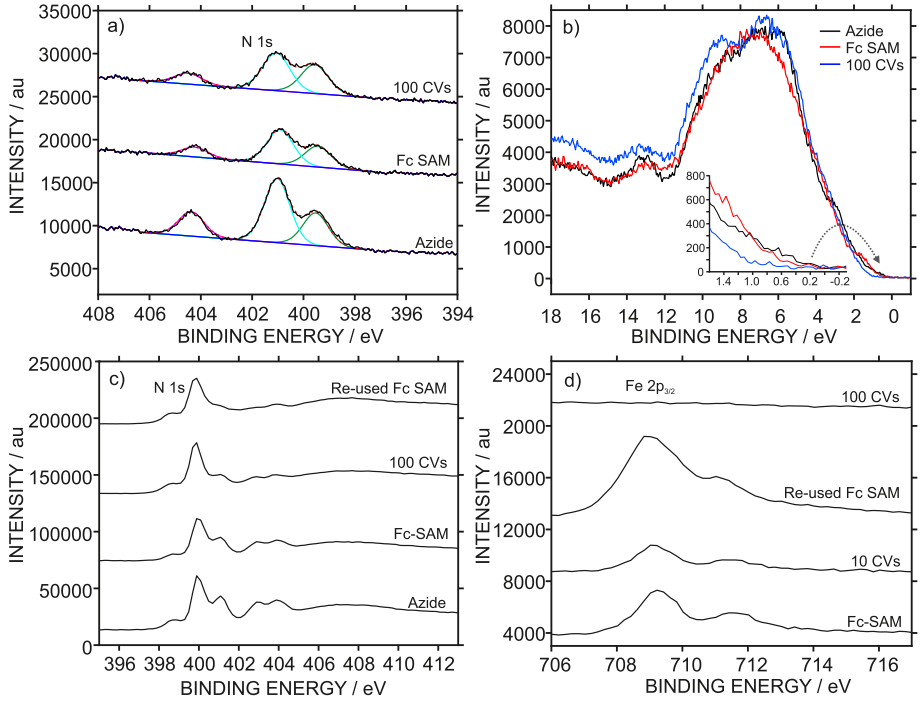

Fig. 2. (a) SR-XPS N 1s core level spectra and (b) VBS and DOS near to the Fermi edge for azide|GC, Fc|azide|GC electrode and Fc|azide|GC electrode subjected to 100 CVs at an expanded potential window in $NaPF_6$ ACN solution. (c) NEXAFS N 1s and (d) Fe $2p_{3/2}$ edge spectra for azide|GC, Fc|azide|GC electrode and Fc|azide|GC electrode subjected to 10 and 100 CVs at an expanded potential window in $NaPF_6$ ACN solution, together with Fc|azide|GC electrode after depositing and removing membrane M2 three consecutive times.

samples. Regarding N 1s spectra, there are four π* resonances at 400, 401, 403 and 404 eV, and two lower energy peaks (about 399.5 and 399.8 eV) that are assigned to the two adjacent nitrogen atoms (π* resonances again) of the azide moiety [48,49]. The small peak at about 398.3 eV is due to X-ray induced decomposition of azide groups into imine and azo functionalities [48], noting that the clicked SAM has been shown to be unstable in the beam. Hence, as stated above, there must be a small amount of unreacted azide (due to steric hindrance effects) on the clicked surface giving rise to the decomposition product peak at 398.3 eV in all cases. The pattern where the π* resonances at about 401, 403 and 404 eV are diminishing and the 400 eV peak is increasing in the clicked films is characteristic of the formation of the 1,2,3-triazole moiety of the clicked SAM [48].

By considering the Fe $2p_{3/2}$ spectra in the Fc|azide|GC, the appearance of a major peak at 709 eV and a minor peak at about 25% of the intensity of the main peak at 711.5 eV are symbolic of Fe^{2+} presence in neutral Fc [49]. However, in samples scanned at a wide potential window, the Fe content significantly diminished from an Fe/N ratio of 0.67 to 0.41 after 10 CVs, whereas it is zero after 100 CVs, signalling the complete removal of the Fe redox center in the monolayer.

3.2. Cation-transfer processes mediated by the developed Fc monolayer

Having inspected the electrochemical behavior of the Fc SAM on a GC electrode, it was a logical extension to explore the addition of a nanometer-thick membrane on top of the SAM, so as to study ion-transfer processes across the membrane|sample interfaces. Hence, it is expected that, if the membrane contains the cation exchanger (Na^+TFPB^-), a cation wave appears during the anodic scan: the oxidized Fc^+ is doped by the anion $TFPB^-$ present in the membrane with the concomitant release of Na^+ to the solution to maintain charge neutrality in the system, as depicted in Fig. 3a. By contrast, when the membrane comprises ETH500 (tetrakis(4-chlorophenyl) borate tetradocecylammonium, dubbed as $TDDA^+TCPB^-$), no exchangeable cation is present and, therefore, the only way to fulfil the electroneutrality of the system is by anions entering from solution (see Fig. 3b). This should be manifested in anion transfer wave in the voltammogram. During the cathodic scan, the contrary processes should occur in both instances.

Fig. 4a (blue line) presents voltammogram in 10 mM NaCl solution with a membrane incorporating NaTFPB (named as M1, Table S3). As hypothesized, a voltammetric peak is displayed as a consequence of the Na^+ transfer across the thin membrane according to the mechanism shown in Fig. 3a. The observed peak is reversible (0.9057 and 0.9254 μC for the cathodic and anodic peak respectively, differing by 2.2%), with $|E_{p,c} - E_{p,a}|$ of 40 mV and 190 mV of $W_{1/2}$. The membrane also displays a thin layer behavior as confirmed by a linearity of the peak current with scan rate (Fig. 4b), and the observed wave is highly reproducible between scans

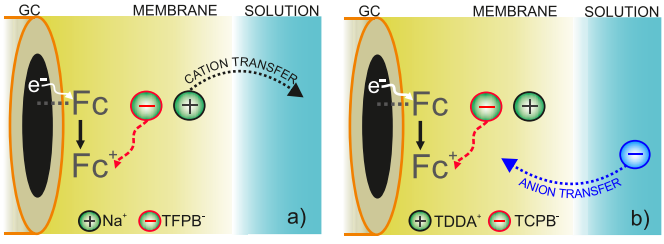

Fig. 3. Illustration of the mechanism for the (a) cation and (b) anion transfer in nanometer-sized membranes.

(Fig. S4a). An excellent reproducibility was found among a set of ten electrodes employing the same membrane: mean absolute deviations of 0.015 μA and 10.76 mV were shown for the anodic peak currents and peak potentials, respectively.

The peak displayed a shift to more positive potentials obeying the Nernst equation with a slope of 59.6 mV/decade change as the concentration of Na^+ is increased from 10 to 60 mM, i.e., from 329.7 mV to 376.1 mV (Fig. 4d). In both cases (i.e., for increasing lipophilicity and concentration), the peak is broader, and the peak current is lower, noting that the integrated charge is not comparable when the peak falls within the region of large capacitance (see for instance the peak for TEA^+ in Fig. 4c).

Through a comparison of the voltammogram for Na^+ transfer with that for the oxidation of the Fc monolayer (see Fig. 4a), it is evident that there is a slight decrease in the peak current (0.74 and 0.60 μA for Fc and Na^+ transfer respectively) while the peak is at least 30 mV broader in the presence of the membrane. As a result, the integrated charge in the anodic part of both peaks differed only by <1% (0.9003 and 0.9057 μC for the Fc monolayer and the Na^+ transfer, respectively). This tends to indicate that the total number of Fc moieties available in the SAM are fully participating in the cation-transfer process of the membrane, which is expected, as the SAM quantity is likely to be the limiting amount or factor. Indeed, the integrated charge remains relatively constant if the amount of NaTFPB in the membrane doubles (M2, Table S3) or even triples (M3, Table S3) when using the same type of monolayer, see Fig. S4b.

The capacitance displayed in the voltammograms of the Fc monolayer also appeared in those involving Na^+ transfer. Before the development of the peak, $|i_{E,a} - i_{E,c}|$ is about the same in both cases (0.27 and 0.24 μA), whereas it remains constant following Na^+ transfer and almost doubles with the Fc|azide|GC electrode (0.46 μA), within the presented potential window (see Fig. 4a). Accordingly, the peak base line is less variable in the case of the Na^+ transfer compared with oxidation of the Fc monolayer (slopes of 0.414 and 0.594 $\mu A V^{-1}$ respectively).

When the Na^+ transfer is studied within a wider potential range, the peak decreases with consecutive scans (Fig. S4c), as is the case with the Fc monolayer (Fig. S2c). Essentially, the gradual alteration of the double-layer capacitance in the Fc monolayer with consecutive scans causes an associated decrease in the Na^+ transfer wave as a consequence of a lower number of Fc moieties available for the transfer process during voltammetry scanning. This effect is totally suppressed if the membrane is scanned within a potential window from −0.2–0.7 V, in which reproducible Na^+ transfer wave is obtained, as presented in Fig. S4a).

The possibility of re-use and replenishment of Fc|azide|GC electrodes after removal of the membrane in THF and deposition of a fresh one was also investigated. Unfortunately, the peak for the Na^+ transfer process gradually diminished with subsequent re-use of the same monolayer (see Fig. S5a). Indeed, the behavior of the Fc|azide|GC electrode in $TBAPF_6$ after three re-uses yielded no peak in the CV voltammogram (see Fig. S5b). There are four principal explanations for this behavior: (i) the Fc monolayer is dissolved in THF; (ii) the activity of the Fc moieties is somehow blocked as a consequence of the electrochemical experiments; (iii) the Fc monolayer is entrapped in such a way in the membrane matrix that it is removed together with the membrane through dissolution in THF; and (iv) some of the membrane components are entrapped in the Fc monolayer and are not removed via THF washing, affecting the re-use of the Fc monolayer.

The first option can be discarded since the voltammograms in $TBAPF_6$ for a freshly prepared Fc monolayer before and after rinsing in an abundant quantity of THF showed no changes (data not shown). Furthermore, the third explanation is more probable than the second one because, if the electrochemical experiments

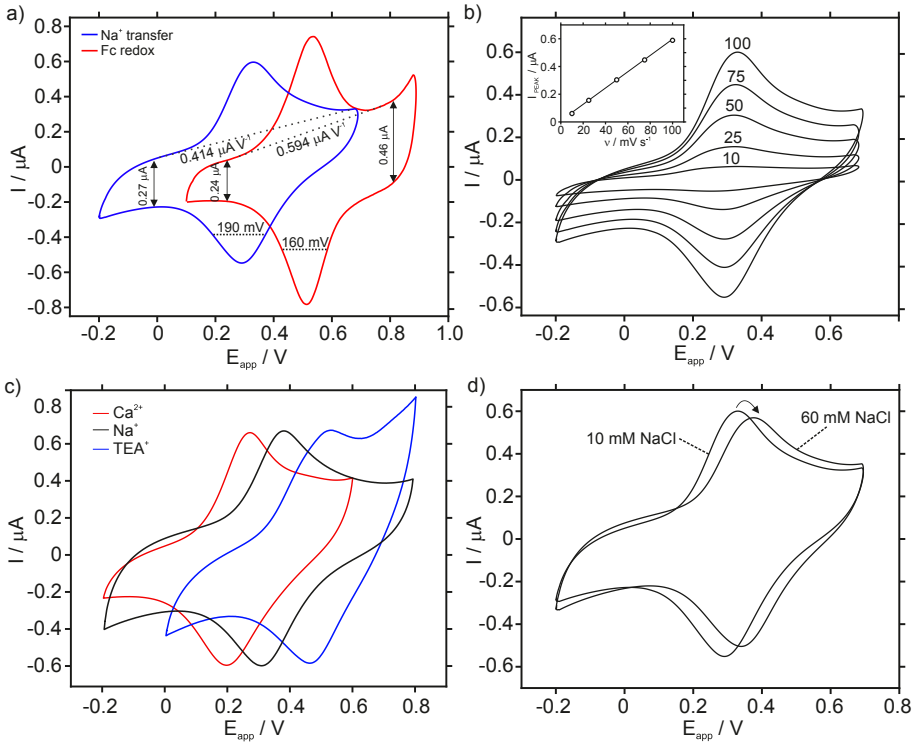

Fig. 4. a) Comparison of the voltammograms displayed by the NaTFPB-based membrane (M1) in 10 mM NaCl with that observed for the Fc|azide|GC electrode in 0.1 M $TBAPF_6$ ACN solution (from Fig. 1c). Scan rate = 100 mV s^{-1}. b) Voltammograms at increasing scan rates in 10 mM NaCl using membrane M1. Inset: linearity of the peak current with the scan rate. c) Voltammograms in 10 mM NaCl, $CaCl_2$ and TEACl using the membrane M1. Scan rate = 100 mV s^{-1}. d) Voltammograms at increasing concentrations of NaCl using membrane M1. Scan rate = 100 mV s^{-1}.

influenced the Fc monolayer, a gradual decrease in the voltammetric peaks and/or irreversible waves would be observed with consecutive scanning, noting that the observed voltammograms were fairly reproducible for successive scans after the initial membrane application (see Fig. S4a). To decide between the third and fourth accounts, extra experiments involving the Fc monolayer surface were deemed essential.

In order to understand the origin of this deterioration of the electrochemical behavior of the Fc monolayer, SR-XPS and NEXAFS experiments were undertaken before and after membrane removal. The results of a Fc|azide|GC electrode in which the membrane had been spin coated and removed three times displayed no diminution in the Fe content of the membrane (see Table S2), highlighting that the decline in electrochemistry is due, not to removal of Fc in the monolayer, but some other phenomenon. In contrast, we detected Cl 2p core level spectra that are symbolic of PVC (Fig. 5a and Table S1) [50], which may be due to an intermingling of PVC polymer chains with the Fc monolayer as a consequence of thermally excited capillary waves. This behavior has been already reported in the literature by De Marco et al. and others [51,52].

Regarding the NEXAFS N1s spectra (Fig. 2c), the main peaks at 399, 400 and 404 eV are maintained. Hence, NEXAFS Fe $2p_{3/2}$ spectra (Fig. 2d) reveals that the Fe redox center is not removed, but it seems to alter it to a mixture of Fe^{2+} and Fe^{3+} with peaks at 707.7 eV (minor peak) and 709.5 eV (major peak) at an intensity ratio of 1:3 [53], along with Fe^{2+} states signified by a major peak at 709 eV and a minor peak at about 25% of the intensity of the main peak at 711.5 eV [49]. Presumably, this is due to a degree of oxidation of the Fc moieties in the SAM by the presence of dissolved oxygen in the THF solvent, noting that it has been demonstrated that ferrocenium cation decompose by both oxygen and water action [54,55].

A depth profile of the membrane|Fc|azide|GC electrode was also measured (see Fig. 5b–d). Over a sputtering timeframe of 55–77 min, it is obvious that the PVC membrane has sputtered through to the Fc monolayer at the buried interface. The membrane|Fc interface is well-defined during the sputtering, while there is evidence of certain degree of melding of the PVC film with the Fc SAM, as evidenced by the broadening of the interface from 385 nm (55 min of sputtering) to 539 nm (77 min of sputtering). The use of a high hydrophobicity polymer membrane (e.g., PU or poly(methyl methacrylate)-poly(decyl methacrylate) [PMMA-PDMA]) is capable of minimizing the influence of thermally excited capillary waves, and may obviate the problem of a blurred and melded interface between the Fc SAM and the polymer [51,52].

The ability of a membrane to be rinsed between measurements while preserving its response was also evaluated. A decrease in the voltammetric signal is observed once the membrane is washed with abundant quantities of water between measurements (see Fig. S6a), which is analogous to the behavior in PVC membranes that are backside contacted with POT [12]. However, once PVC is replaced by PU (membranes M4-M6, Table S3), very reproducible voltammograms are observed after abundant rinsing with water (Fig. S6b). Interestingly, the use of PU has permitted a significant reduction in the amount of plasticizer in the membrane with no drastic changes in the voltammetric response, also improving the hemo-and-biocompatibility of the membrane in view of further analytical applications [56]. Presumably, this is due to suppressed leaching of the plasticizer and associated ion sensor ingredients on continuous exposure to aqueous media.

3.3. Comparison with other systems reported to assist cation transfer

By consideration of Fc|azide|GC with other electrodes based on

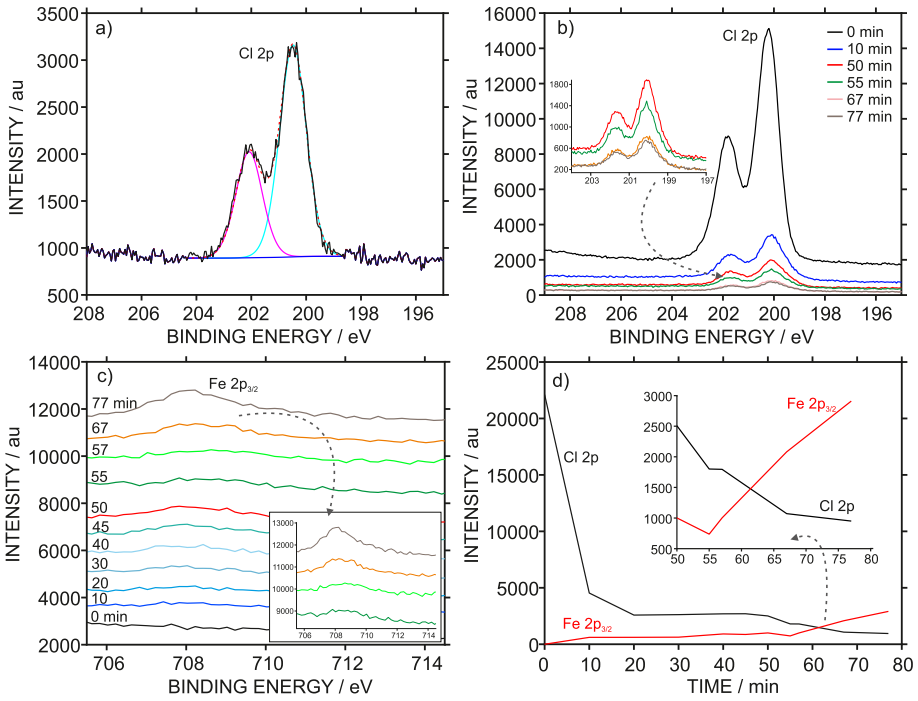

Fig. 5. (a) SR-XPS Cl 2p core level spectrum for the Fc|azide|GC after the deposition and removal (3 times) of membrane M1. (b) SR-XPS Cl 2p overlay spectra during depth profiling of the membrane|Fc|azide|GC involving Ar ion sputtering. (c) NEXAFS Fe $2p_{3/2}$ overlay spectra during the depth profiling of the membrane|Fc|azide|GC. (d) Depth profile for Cl 2p and Fe $2p_{3/2}$. Sputtering rate of 12 ± 1 nm min^{-1} at 25 mA scales to 7 nm min^{-1} at 15 mA, which indicates that the buried interface spreads over a depth of 385–525 nm [59]. Membrane = M1.

voltammetric thin membranes published for cation detection (i.e., electrodes based on POT [11,13] as well as Os(II)/(III) [16] or helicenes [17,18] directly dissolved in the membrane) Table S4 lists the main features associated with the electrochemical behavior of the redox-active mediator as well as Na^+ transfer in membranes comprising NaTFPB. Importantly, both Os- and helicene-based compounds showed an electrochemical behavior in organic solution that closely involves one electron transfer reaction ($W_{1/2}$ is 100 and 59 mV, respectively) [16–18]. However, electroactive films of POT [19] and the Fc monolayer (this paper) display broader peaks due to two probable reasons: (i) inhomogeneity of the film resulting in multiple standard potentials, thereby generating a charge distribution over the entire surface and/or (ii) kinetic limitations inherent to the film conformation during redox changes [19].

Regarding the oxidation potential, POT and Os compounds present more positive values, with helicenes showing the lowest values, whereas a Fc monolayer gives rise to an intermediate value of 540 mV (see Table S4). This value is very convenient in order to avoid side reactions happening at positive potentials that may interfere with the ion-transfer process. Furthermore, reversibility is excellent with the Fc monolayer as evidenced by a reduced peak separation compared with the three other mediators.

In the case of POT, the available charge for the mediation of ion transfer is <30% with a membrane containing 40 mmol kg^{-1} of NaTFPB (see Table S4) [11]. Although the use of a higher amount of NaTFPB in the membrane produces a higher useable charge, a high amount of NaTFPB is incommensurate with a view to the incorporation of ionophores in the membrane. By contrast, as mentioned above, a composition embodying 40 mmol kg^{-1} NaTFPB is sufficient to oxidize entirely the Fc moieties of the SAM in GC|SAM|membrane, which is convenient towards assisted ion transfer via a selective process.

On the other hand, with Os and helicene compounds dissolved in the membrane, a minimum amount of the compound is required to provide an acceptable peak shape, high peak current, narrow peak width and reversible peaks [16–18]. At elevated amounts of redox mediator in the membrane, a higher concentration of NaTFPB is required to promote cation transfer, which is a double drawback since the incorporation of a cation ionophore will necessitate a high loading of these expensive reagents, and a marked leaching of membrane components occurs under these conditions. For example, a membrane based on 92 mmol kg^{-1} of helicene and 280 mmol kg^{-1} of NaTFPB presenting appropriate peaks for Na^+ transfer (see Table S4) [17] necessitates the incorporation of a double amount of Na ionophore (i.e. 560 mmol kg^{-1}), which is the traditional composition used in potentiometry with POT-based electrodes. However, Jarolimova et al. presented a distinct membrane composition comprising instead 60 mmol kg^{-1} of helicene, 92 mmol kg^{-1} of NaTFPB and 175 mmol kg^{-1} of the Na ionophore [17]. Although the amounts of the membrane components are reduced compared to the expected ones, the authors claim that a gradual loss of active membrane components in the sample solution renders the system inadequate for the selective detection of cations. The use of immobilized redox-active molecules in a film at the buried interface of the membrane (as it is the case of POT and Fc SAM) enables a usage of much smaller amounts of compounds, thereby reducing/supressing the process of membrane leaching, and it is in principle far more compatible with an incorporation of ionophores in membranes. This is a clear advantage compared with the use of Os and helicene compounds in the membrane [16–18].

3.4. Anion-transfer processes mediated by the developed Fc monolayer

Voltammograms for different anions employing a membrane based on ETH500 (M7, Table S3) are presented in Fig. 6a. The peak position follows the Hofmeister series ($PF_6^- < ClO_4^- < NO_3^-$), as

expected when there is no ionophore in the membrane. In addition, the peak shifts to less positive potentials in accordance with the Nernst equation for increasing concentrations of these anions, noting that peak broadening and de-intensification are evident at low concentrations with peak potentials >0.7 V. As an example, calibration graphs for ClO_4^- and PF_6^- are shown in Fig. 6b and Fig. S7a respectively.

Significantly, the observed voltammogram with Cl^- displayed no voltammetric peak within the applied potential window (see Fig. 6a). However, with an expanded potential window (0.1–1.5 V, Fig. S8), an anodic irreversible peak appears at about 1.4 V in the first voltammetric scan, although the peak is absent in successive scans. This irreversibility is probably associated with the double-layer capacitance in the Fc monolayer appearing at the same potential range of chloride ion transfer.

The reported peak for Cl^- using membranes based on the helicene compound apparently showed reversible peaks [18]. This is not the case with the Os compound, although the observed peak was totally reproducible in voltammetric cycling, as the solution acts as a larger reservoir of the anion [16]. Concerning the other characteristics of Cl^- peaks using the aforesaid systems, the peak current is higher when using the Os compound because of its higher loading in the membrane (see Table S4). The Cl^- peak using both systems displayed similar widths for the anodic peaks, but the $|E_{p,c} - E_{p,a}|$ is much higher with the Os compound (cf., 250 mV *versus* 60 mV). Additionally, this value is variable with different anions revealing distinct peak shapes. As a trend, the more lipophilic the anion, the closer the peak is to the ideal Gaussian wave [16]. Notwithstanding, it was demonstrated that this behavior is not related to the presence of an ohmic drop in the electrode, and it seems to be consistent with thermodynamic and/or kinetic factors inherent to the ion-transfer processes of the membrane|sample interface [16]. Importantly, our Fc-based electrode displayed the same performance with different anions, as was noted above (see Fig. 6a).

Variation of the amount of ETH500 in the membrane (M7-M9, Table S3) did not alter significantly the voltammograms in 10 mM $NaPF_6$ (see Fig. S7b). As was the case with membrane M1 comprising NaTFPB, the limiting factor on the anion transfer peak, as evidenced by the charge under the peak, is the amount of oxidized/reduced Fc molecules in the SAM. Hypothetically, if the amount of NaTFPB (in M1) or ETH500 (in M7) is gradually reduced, there will be a certain point when the current of the voltammetric peak will be reduced, which is not useful for the purpose of detecting cations and anions, so this aspect was not further investigated.

3.5. Incorporation of selective ionophores in the nanometer-sized membrane

Having demonstrated both cation and anion-transfer processes with the developed membrane|Fc|azide|GC electrode by tuning the membrane composition, the incorporation of either a cation or anion ionophore in the membrane was further investigated. Fig. 7 shows voltammograms for increasing concentrations of Li^+ and Cl^- using membranes M10 and M11 (see Table S3) based on lithium and chloride [57] ionophores, respectively. The Li^+ peak shifts to positive potentials and the Cl^- one to negative values as a function of concentration of the primary ion, both in accordance with the Nernst equation (see the inset plots). The observed limits of detection ($10^{-5.7}$ and $10^{-4.9}$ M for Li^+ and Cl^-, respectively) and linear ranges ($10^{-4.8}$–10^{-2} M and 10^{-4}–10^{-1} M, respectively) agree with those reported with these ionophores in conventional potentiometric membrane sensors [57,58].

It is advantageous that the observed voltammograms in the aforesaid cases fall within a potential range before the appearance of the region of increasing current in the corresponding electrode. However, this may not be the case with all ionophores and, in addition, the potential at which this region sets in may vary with different membrane compositions.

For example, the voltammetric peaks for Na^+ and K^+ using membrane M12 (Table S3) employing a potassium ionophore (a highly selective one) are presented in Fig. S9. The peaks for Na^+ (background electrolyte) and K^+ (at 605 and 930 mV, respectively) are manifested as a shoulder on the baseline, similar to the behavior noted with TBA^+ and membrane M1 (see Fig. 4c). Despite this unusual peak shape, the logarithmic selectivity coefficient of the membrane towards Na^+ with K^+ as the primary ion can be calculated from the peak separation. Accordingly, a value of $logK_{Na,K} = -5.4$ is obtained for the valinomycin-based membrane, which is consistent with values determined by traditional potentiometry as well as thin membranes that are backside contacted with POT [13]. This is apparently indicative of the ionophore functioning correctly, but the voltammetric peak has an inappropriate shape as it lies in the region of the increasing current in the Fc monolayer.

With anion-ionophores, given that, in principle, the potential range of the anion-transfer peak should not overlap with the voltammetric baseline that coincides with the region of the increasing current as the case of chloride, it is expected that an anion-ionophore with a sufficiently high selectivity for the target will present a peak potential window (displaced to less positive values) that reveals the entire calibration curve, as with low-selectivity

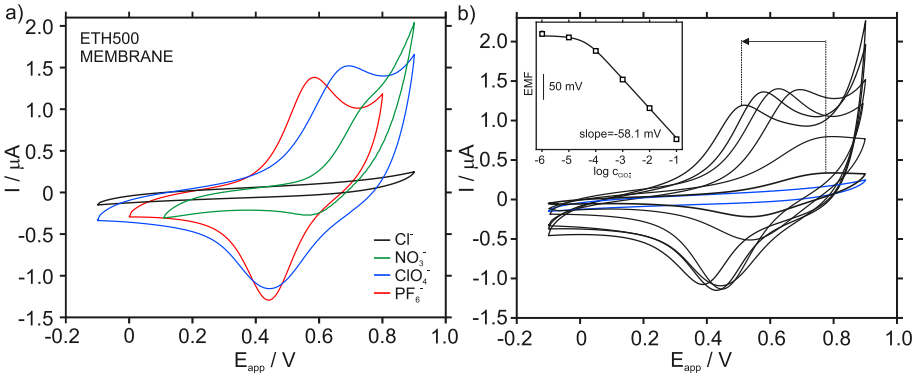

Fig. 6. (a) Voltammograms with membrane M7 in 10 mM solution of the sodium salts of different anions. (b) Response at increasing $NaClO_4$ concentration in 1 mM NaCl background (blue curve). Inset = calibration curve. Scan rate = 100 mV s^{-1}. (For interpretation of the references to color in this figure legend, the reader is referred to the Web version of this article.)

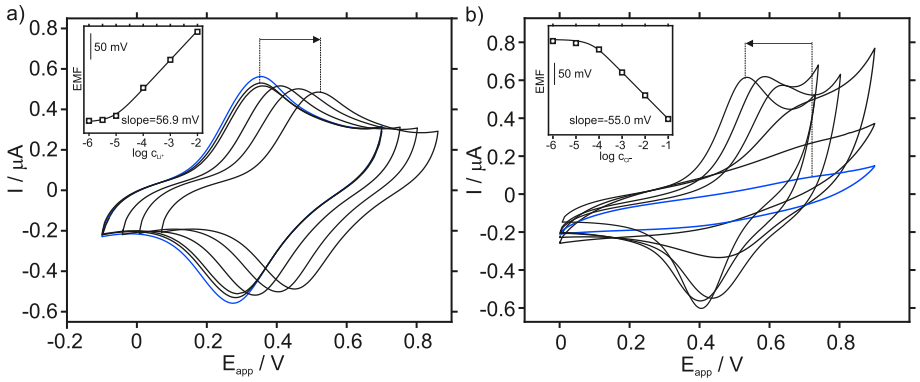

Fig. 7. Calibration graphs observed for (a) lithium and (b) chloride ions using membranes M10 and M11, respectively. The blue curves correspond to the background electrolyte (1 mM NaCl and 1 mM $NaNO_3$ respectively). Scan rate = 100 mV s^{-1}. (For interpretation of the references to color in this figure legend, the reader is referred to the Web version of this article.)

cation ionophores.

As a demonstration of the analytical utility of the developed Fc-based sensor, lithium was detected in human urine and chloride was analyzed in different drinking waters using the standard addition approach. Table S5 presents the analytical data with different samples. As an example, the voltammograms at increasing concentrations of Li^+ in urine are presented in Fig. S10. Lithium recoveries were between 90 and 110%, and there was a good agreement between the detected and labelled chloride concentrations in the water samples. These excellent analytical results highlight the potential of the developed sensors for the analysis of real samples.

4. Conclusions

Ferrocene monolayer on glassy carbon electrode successfully mediates for the first time both cation and anion transfer across nanometer-sized membranes. For this purpose, the membrane composition is tuned: the presence of a cation exchanger allows for cation transfer, whereas a lipophilic salt promotes anion transfer. As the ion concentration increases in the bulk of the sample solution, the peak position of the voltammograms displayed by these membranes follows a Nernstian behavior. However, the appearance of a double-layer capacitance in the Fc SAM is manifested in a large current increase that influences the peak shape for the voltammetric ion transfer when the membrane is deposited on top of the monolayer. Thus, we found that this large current overlaps with the ion-transfer peak in some specific cases: (i) for very lipophilic cations (such as TBA^+), (ii) anions of certain hydrophilicity (NO_3^- and so on), and (iii) membranes based on either a high selectivity cation ionophore or low selectivity anion ionophore. Advantageously, assisted ion transfer with membranes doped with lithium and chloride ionophores has been demonstrated. Indeed, analytical detection of these two ions in real samples (human urine and drinking water) has been presented as proof-of-concept of the applicability of the developed electrodes. Further work will involve a systematic investigation of substrates and immobilized metallic centers with the aim of expanding the potential window for the ion-transfer processes in these systems. Overall, a covalently attached redox molecule as mediator of ion transfer across voltammetry nanometer-sized membranes shows a series of advantages over other systems published before (i.e. it averts the leaching of membrane components, prevents from chloride interference and allows for easy incorporation of certain ionophores).

Acknowledgments

The authors acknowledge the financial support of the European Union (Marie Skłodowska-Curie Individual Fellowship European, H2020-MSCA–IF–2017, Grant no. 792824), KTH Royal Institute of Technology (Starting Grant Programme, K-2017-0371), Swedish Research Council (Project Grant VR-2017-4887) and the Wenner-Gren Foundation (Scholarship UPD2017-0220). We are grateful for the support of the European Community's Seventh Framework Programme (FP7/2007-2013) under grant agreement n 312284 for research that was conducted on the Materials Science Beamline (MSB) at the Elettra Synchrotron. We thank Prof. Licheng Sun for the scientific assistance in the preparation of the monolayer. Special acknowledge to Drs. Nataliya Tsud and Kevin C. Prince at Elettra Synchrotron for assistance with the experiments. We also thank Dr. Bradley for his help with the measurements at the Elettra Synchrotron and fruitful discussions. MC and GAC acknowledge the CERIC users' grant for the travel funding to visit Elettra Synchrotron.

Appendix A. Supplementary data

Supplementary data to this article can be found online at https://doi.org/10.1016/j.electacta.2019.05.091.

References

[1] G.A. Crespo, E. Bakker, Dynamic electrochemistry with ionophore based ion-selective membranes, RSC Adv. 3 (2013) 25461–25474.
[2] M. Cuartero, G.A. Crespo, E. Bakker, Thin layer samples controlled by dynamic electrochemistry, Chimia 69 (2015) 203–206.
[3] E. Zdrachek, E. Bakker, Potentiometric sensing, Anal. Chem. 91 (2019) 2–26.
[4] J. Zhang, A.R. Harris, R.W. Cattrall, A.M. Bond, Voltammetric ion-selective electrodes for the selective determination of cations and anions, Anal. Chem. 82 (2010) 1624–1633.
[5] A.R. Harris, J. Zhang, R.W. Cattrall, A.M. Bond, Applications of voltammetric ion selective electrodes to complex matrices, Anal Meth UK 5 (2013) 3840–3852.
[6] M.B. Garada, B. Kabagambe, Y. Kim, S. Amemiya, Ion-transfer voltammetry of perfluoroalkanesulfonates and perfluoroalkanecarboxylates: picomolar detection limit and high lipophilicity, Anal. Chem. 86 (2014) 11230–11237.
[7] B. Kabagambe, M.B. Garada, R. Ishimatsu, S. Amemiya, Subnanomolar detection limit of stripping voltammetric Ca^{2+}-selective electrode: effects of analyte charge and sample contamination, Anal. Chem. 86 (2014) 7939–7946.
[8] B. Kabagambe, A. Izadyar, S. Amemiya, Stripping voltammetry of nanomolar potassium and ammonium ions using a valinomycin-doped double-polymer electrode, Anal. Chem. 84 (2012) 7979–7986.
[9] Y. Kim, S. Amemiya, Stripping analysis of nanomolar perchlorate in drinking water with a voltammetric ion-selective electrode based on thin-layer liquid membrane, Anal. Chem. 80 (2008) 6056–6065.
[10] P.C. Si, E. Bakker, Thin layer electrochemical extraction of non-redoxactive cations with an anion-exchanging conducting polymer overlaid with a

selective membrane, Chem. Commun. (2009) 5260–5262.
[11] G.A. Crespo, M. Cuartero, E. Bakker, Thin layer ionophore-based membrane for multianalyte ion activity detection, Anal. Chem. 87 (2015) 7729–7737.
[12] M. Cuartero, G.A. Crespo, E. Bakker, Polyurethane ionophore-based thin layer membranes for voltammetric ion activity sensing, Anal. Chem. 88 (2016) 5649–5654.
[13] M. Cuartero, G.A. Crespo, E. Bakker, Ionophore-based voltammetric ion activity sensing with thin layer membranes, Anal. Chem. 88 (2016) 1654–1660.
[14] M. Cuartero, R.G. Acres, J. Bradley, Z. Jarolimova, L. Wang, E. Bakker, G.A. Crespo, R. De Marco, Electrochemical mechanism of ferrocene-based redox molecules in thin film membrane electrodes, Electrochim. Acta 238 (2017) 357–367.
[15] M. Sohail, R. De Marco, Z. Jarolimova, M. Pawlak, E. Bakker, N. He, R.M. Latonen, T. Lindfors, J. Bobacka, Transportation and accumulation of redox active species at the buried interfaces of plasticized membrane electrodes, Langmuir 31 (2015) 10599–10609.
[16] S. Jansod, L. Wang, M. Cuartero, E. Bakker, Electrochemical ion transfer mediated by a lipophilic Os(II)/Os(III) dinonyl bipyridyl probe incorporated in thin film membranes, Chem. Commun. 53 (2017) 10757–10760.
[17] Z. Jarolimova, J. Bosson, G.M. Labrador, J. Lacour, E. Bakker, Ion transfer voltammetry at thin films based on functionalized cationic 6 helicenes, Electroanalysis 30 (2018) 650–657.
[18] Z. Jarolimova, J. Bosson, G.M. Labrador, J. Lacour, E. Bakker, Ion transfer voltammetry in polyurethane thin films based on functionalised cationic 6 helicenes for carbonate detection, Electroanalysis 30 (2018) 1378–1385.
[19] M. Cuartero, R.G. Acres, R. De Marco, E. Bakker, G.A. Crespo, Electrochemical ion transfer with thin films of poly(3-octylthiophene), Anal. Chem. 88 (2016) 6939–6946.
[20] G.A. Crespo, S. Macho, F.X. Rius, Ion-selective electrodes using carbon nanotubes as ion-to-electron transducers, Anal. Chem. 80 (2008) 1316–1322.
[21] B. Paczosa-Bator, L. Cabaj, M. Ras, B. Bas, R. Piech, Potentiometric sensor platform based on a carbon black modified electrodes, Int. J. Electrochem. Sci. 9 (2014) 2816–2823.
[22] R.S. Bowen, D.R. Picard, S. Verberne-Sutton, C.J. Brame, Incorporating student design in an HPLC lab activity student metacognition and argumentation, J Chem. Educ. 95 (2018) 108–115.
[23] J.B. Hu, X.U. Zou, A. Stein, P. Buhlmann, Ion-selective electrodes with colloid-imprinted mesoporous carbon as solid contact, Anal. Chem. 86 (2014) 7111–7118.
[24] M. Zhou, S.Y. Gan, B. Cai, F.H. Li, W.G. Ma, D.X. Han, L. Niu, Effective solid contact for ion-selective electrodes: tetrakis(4-chlorophenyl)borate (TB-) anions doped nanocluster films, Anal. Chem. 84 (2012) 3480–3483.
[25] E. Jaworska, M. Wojcik, A. Kisiel, J. Mieczkowski, A. Michalska, Gold nanoparticles solid contact for ion-selective electrodes of highly stable potential readings, Talanta 85 (2011) 1986–1989.
[26] M. Fibbioli, K. Bandyopadhyay, S.G. Liu, L. Echegoyen, O. Enger, F. Diederich, P. Buhlmann, E. Pretsch, Redox-active self-assembled monolayers as novel solid contacts for ion-selective electrodes, Chem. Commun. (2000) 339–340.
[27] M. Fibbioli, K. Bandyopadhyay, S.G. Liu, L. Echegoyen, O. Enger, F. Diederich, D. Gingery, P. Buhlmann, H. Persson, U.W. Suter, E. Pretsch, Redox-active self-assembled monolayers for solid-contact polymeric membrane ion-selective electrodes, Chem. Mater. 14 (2002) 1721–1729.
[28] C. Gabrielli, P. Hemery, P. Liatsi, M. Masure, H. Perrot, An electrogravimetric study of an all-solid-state potassium selective electrode with Prussian blue as the electroactive solid internal contact, J. Electrochem. Soc. 152 (2005) H219–H224.
[29] J. Tan, J.H. Bergantin, A. Merkoci, S. Alegret, F. Sevilla, Oil dispersion of AgI/Ag2S salts as a new electroactive material for potentiometric sensing of iodide and cyanide, Sensor. Actuator. B Chem. 101 (2004) 57–62.
[30] X.U. Zou, J.H. Cheong, B.J. Taitt, P. Buhlmann, Solid contact ion-selective electrodes with a well-controlled Co(II)/Co(III) redox buffer layer, Anal. Chem. 85 (2013) 9350–9355.
[31] E. Jaworska, M.L. Naitana, E. Stelmach, G. Pomarico, M. Wojciechowski, E. Bulska, K. Maksymiuk, R. Paolesse, A. Michalska, Introducing cobalt(II) porphyrin/cobalt(III) corrole containing transducers for improved potential reproducibility and performance of all-solid-state ion-selective electrodes, Anal. Chem. 89 (2017) 7107–7114.
[32] J.B. Hu, A. Stein, P. Buhlmann, Rational design of all-solid-state ion-selective electrodes and reference electrodes, TRAC 76 (2016) 102–114.
[33] S.B. Sek, R. Bilewicz, E. Grygolowicz-Pawlak, I. Grudzien, Z. Brzozka, E. Malinowska, Design of ferrocene organothiol monolayer as intermediate phase for miniaturized electrochemical sensors with gold contact, Pol. J. Chem. 78 (2004) 1655–1665.
[34] E. Grygolowicz-Pawlak, K. Wygladacz, S. Sek, R. Bilewicz, Z. Brzozka, E. Malinowska, Studies on ferrocene organothiol monolayer as an intermediate phase of potentiometric sensors with gold inner contact, Sensor. Actuator. B Chem. 111 (2005) 310–316.
[35] Y. Yang, M. Cuartero, V.R. Goncales, J.J. Gooding, E. Bakker, Light-addressable ion sensing for real-time monitoring of extracellular potassium, Angew. Chem. Int. Ed. 57 (2018) 16801–16805.
[36] D. Evrard, F. Lambert, C. Policar, V. Balland, B. Limoges, Electrochemical functionalization of carbon surfaces by aromatic azide or alkyne molecules: a versatile platform for click chemistry, Chem. Eur J. 14 (2008) 9286–9291.
[37] L.P. Tong, M. Gothelid, L.C. Sun, Oxygen evolution at functionalized carbon surfaces: a strategy for immobilization of molecular water oxidation catalysts, Chem. Commun. 48 (2012) 10025–10027.
[38] J.F. Smalley, S.W. Feldberg, C.E.D. Chidsey, M.R. Linford, M.D. Newton, Y.P. Liu, The kinetics of electron-transfer through ferrocene-terminated alkanethiol monolayers on gold, J Phys Chem-US 99 (1995) 13141–13149.
[39] G.K. Rowe, M.T. Carter, J.N. Richardson, R.W. Murray, Consequences of kinetic dispersion on the electrochemistry of an adsorbed redox-active monolayer, Langmuir 11 (1995) 1797–1806.
[40] A.L. Eckermann, D.J. Feld, J.A. Shaw, T.J. Meade, Electrochemistry of redox-active self-assembled monolayers, Coord. Chem. Rev. 254 (2010) 1769–1802.
[41] S. Ciampi, M. James, M.H. Choudhury, N.A. Darwish, J.J. Gooding, The detailed characterization of electrochemically switchable molecular assemblies on silicon electrodes, Phys. Chem. Chem. Phys. 15 (2013) 9879–9890.
[42] E. Laviron, Use of linear potential sweep voltammetry and of Ac voltammetry for the study of the surface electrochemical reaction of strongly adsorbed systems and of redox modified electrodes, J. Electroanal. Chem. 100 (1979) 263–270.
[43] A. Bensghaier, Z. Salmi, B. Le Droumaguet, A. Mekki, A.A. Mohamed, M. Beji, M.M. Chehimi, A Diazonium interface chemistry and click polymerization: a novel route for carbon nanotube-polytriazole nanocomposites, Surf. Interface Anal. 48 (2016) 509–513.
[44] M. Coates, H. Elamari, C. Girard, S. Griveau, T. Nyokong, F. Bedioui, 4-Azidoaniline-based electropolymer as a building block for functionalisation of conductive surfaces, J. Electroanal. Chem. 670 (2012) 79–84.
[45] A.N. Titov, Y.M. Yarmoshenko, P. Bazylewski, M.V. Yablonskikh, E.Z. Kurmaev, R. Wilks, A. Moewes, V.A. Tsurin, V.V. Fedorenko, O.N. Suvorova, S.Y. Ketkov, M. Neumann, G.S. Chang, Charge transfer and band gap of ferrocene intercalated into TiSe2, Chem. Phys. Lett. 497 (2010) 187–190.
[46] N. Soin, S.S. Roy, S. Roy, K.S. Hazra, D.S. Misra, T.H. Lim, C.J. Hetherington, J.A. McLaughlin, Enhanced and stable field emission from in situ nitrogen-doped few-layered graphene nanoflakes, J. Phys. Chem. C 115 (2011) 5366–5372.
[47] S.J. Wang, H.H. Park, Study of PEDOT : PSS-SnO2 nanocomposite film as an anode for polymer electronics, J. Electroceram. 18 (2007) 161–165.
[48] E. Darlatt, A. Nefedov, C.H.H. Traulsen, J. Poppenberg, S. Richter, P.M. Dietrich, A. Lippitz, R. Illgen, J. Kuhn, C.A. Schalley, C. Woll, W.E.S. Unger, Interpretation of experimental N K NEXAFS of azide, 1,2,3-triazole and terpyridyl groups by DFT spectrum simulations, J Electron Spectrosc 185 (2012) 621–624.
[49] E. Otero, N. Kosugi, S.G. Urquhart, Strong double excitation and open-shell features in the near-edge x-ray absorption fine structure spectroscopy of ferrocene and ferrocenium compounds, J. Chem. Phys. 131 (2009).
[50] J.F. Moulder, W.F. Stickle, P.E. Sobol, K.D. Bombden, Handbook of X-Ray Photoelectron Spectroscopy, 1992.
[51] J.P. Veder, R. De Marco, G. Clarke, S.P. Jiang, K. Prince, E. Pretsch, E. Bakker, Water uptake in the hydrophilic poly(3,4-ethylenedioxythiophene):poly(-styrene sulfonate) solid-contact of all-solid-state polymeric ion-selective electrodes, Analyst 136 (2011) 3252–3258.
[52] M. Sferrazza, M. Heppenstall-Butler, R. Cubitt, D. Bucknall, J. Webster, R.A.L. Jones, Interfacial instability driven by dispersive forces: the early stages of spinodal dewetting of a thin polymer film on a polymer substrate, Phys. Rev. Lett. 81 (1998) 5173–5176.
[53] F. Zheng, V. Perez-Dieste, J.L. McChesney, Y.Y. Luk, N.L. Abbott, F.J. Himpsel, Detection and switching of the oxidation state of Fe in a self-assembled monolayer, Surf. Sci. 587 (2005) L191–L196.
[54] A. Singh, D.R. Chowdhury, A. Paul, A kinetic study of ferrocenium cation decomposition utilizing an integrated electrochemical methodology composed of cyclic voltammetry and amperometry, Analyst 139 (2014) 5747–5754.
[55] R.A. Wong, Y. Yokota, M. Wakisaka, J. Inukai, Y. Kim, Discerning the redox-dependent electronic and interfacial structures in electroactive self-assembled monolayers, J. Am. Chem. Soc. 140 (2018) 13672–13679.
[56] G.S. Cha, D. Liu, M.E. Meyerhoff, H.C. Cantor, A.R. Midgley, H.D. Goldberg, R.B. Brown, Electrochemical performance, biocompatibility, and adhesion of new polymer matrices for solid-state ion sensors, Anal. Chem. 63 (1991) 1666–1672.
[57] N. Pankratova, M. Cuartero, L.A. Jowett, E.N.W. Howe, P.A. Gale, E. Bakker, G.A. Crespo, Fluorinated tripodal receptors for potentiometric chloride detection in biological fluids, Biosens. Bioelectron. 99 (2018) 70–76.
[58] M. Novell, T. Guinovart, P. Blondeau, F.X. Rius, F.J. Andrade, A paper-based potentiometric cell for decentralized monitoring of Li levels in whole blood, Lab Chip 14 (2014) 1308–1314.
[59] M. Cuartero, J. Bishop, R. Walker, R.G. Acres, E. Bakker, R. De Marco, G.A. Crespo, Evidence of double layer/capacitive charging in carbon nanomaterial-based solid contact polymeric ion-selective electrodes, Chem. Commun. 52 (2016) 9703–9706.